Comparative performance analysis of Cs_2TiX_6 (X=Br^-, Cl^-, I^-) lead-free perovskite solar cells incorporating single, double and triple layer halides by SCAPS -1D

Arslan Ashfaq[a], Sofia Tahir[a*] Shammas Mushtaq[a], Rania Saleh Alqurashi[c], Muhammad Haneef[a], N. Almousa[d], Ubaid–ur-Rehman[e], Ruy Sebastian Bonilla[b],*

[a]*Department of Physics, Government College University, Faisalabad, 38000, Pakistan*
[b]*Department of Materials, University of Oxford, OX1-3PH, United Kingdom*
[c]*Physics Department, Collage of Science, Al-Baha University, Alaqiq, 65779-7738, Saudi Arabia*
[d]*Department of Physics, College of Science, Princess Nourah Bint Abdulrahman University, P.O.Box 84428, Riyadh,11671, Saudi Arabia*
[e]*Institute of Physics, Polish Academy of Sciences, Al. Lotnikow 32/46, 02-668 Warsaw, Poland*

[*]Corresponding Authors: arslan.ashfaq201@gmail.com (*Arslan Ashfaq),*

sofetahir@gmail.com (*Sofia Tahir)*

Halide perovskites have risen in popularity as appealing light absorber materials, owing primarily to their wide range of applications in solar cells, lasers, photodetectors. However, lead-containing perovskites have the potential to cause substantial environmental damage. As a result, there is a significant need to produce environmentally acceptable lead-free perovskites. In this work, we studied the single, double and triple halides perovskite by numerical simulator SCAPS-1D for maximum performance. We have optimized the absorber layer thickness, $N_A/N_D/N_t$ and interface defect density, back contact electrodes, and temperature effects in a single absorber layer structure. Further, we have optimized the double and triple-layer absorbers for perovskite solar cell structures. The maximum efficiency achieved in the double halide perovskite solar cell is V_{OC} = 1.54 V, J_{SC} = 24.04 mA/cm^2, FF = 82.72 %, and PCE = 30.06 %. Such performance is due to the absorption coefficient spectrum with a wide range of energy band gaps. This has proved its suitability for photovoltaic devices. Overall, our findings reveal that Cs_2TiX_6 (X = Br, Cl, I) Pb-free perovskites have promising and potential features for device performance.

Keywords: Cs_2TiBr_6, Cs_2TiCl_6, Cs_2TiI_6 perovskite, inorganic HTL & ETL, SCAPS-1D

1 Introduction

In recent years, organic-inorganic hybrid perovskite solar cells (PSC) have received a lot of interest due to their remarkable optical and electrical characteristics [1]. PSCs have a maximum conversion efficiency of more than 30 %, beating numerous other types of 3rd generation photovoltaic cells [2, 3]. After traditional silicon solar cells, perovskites emerge as the most promising contender for the next generation of devices. The main issues for the commercialization of conventional ABX_3 structures with cation (A) = $(NH_2)_2CH$ (FA), CH_3NH_3 (MA), Cs, metal (B) = Ti, Sn, Pb, and halide (X) = Br, Cl, I, are toxicity and stability. Their band gap is tunable between 1.2 - 2.3 eV via changing the composition of cation, metal and halide [4]. Titanium is a key component in lead-free PSCs because it has a comparable valence and diameter to lead. This led researchers to replace lead with titanium to create $ATiX_3$ perovskite films [5]. The titanium-based structure is most stable than other perovskite structures. Titanium is earth-abundant, biocompatible, thermally stable and nontoxic [6].

The organic materials in the absorber layer, or used as electron and hole transport layer, also suffer from instability in the presence of environmental moisture, light and oxygen [7]. Furthermore, numerous organic charge transfer materials react with the absorber material, exhibiting hostile behaviour due to hygroscopic features, and are expensive to prepare [8]. In order to overcome these drawbacks, scholars are looking forward to inorganic charge transfer materials which offer improved transparency in the ultraviolet, infrared, and visible spectrums, as well as chemical stability, superior thermal properties, high charge carrier mobility, wide bandgap, and a simple synthesis process [9].

The experimental synthesis and theoretical prediction of lead-free Cs_2TiX_6: X = Br^-, Cl^-, I^- based PSCs have shown changes in the band gap and vacancy-ordered structures [10, 11]. These materials can be used in stable and highly efficient PSC. The theoretical performance of $CsTiBr_6$

based PSC using hole and electron transport material such as $CuSbS_2$ and La doped $BaSnO_3$ was investigated at 29.13 % [12], which is higher than Pb-based PSC. Our group also studied the theory of the $CsTiBr_6$-based PSC using the different hole and electron transport material, doping density, interface layers, back contact and temperature effect (under review). We have optimized the best electron and hole transport material for $CsTiBr_6$-based PSC due to the maximum electron and hole extraction from the absorber layer with lower energy level mismatch between HOMO and VBM.

In this study, we have found an optimized electron transport material (IZGO) and hole transport material ($CuSbS_2$) for PSCs. These HTL and ETL show excellent band alignment with the absorber layer. We have investigated the single, double and triple-layered perovskite absorbers with different thicknesses, doping concentrations and interface layers. We reached an optimized perovskite solar cell with high efficiency by a combination of a single, double and triple layer of absorber material. We report the PVSc performance parameters, including open circuit voltage (V_{OC}), short circuit current density (J_{SC}), fill factor (FF), and power conversion efficiency (PCE), which will aid in designing stable and environmentally friendly Ti-based cells for future exploitation.

2 Simulation Structure

The simulated PSC with a single, double and triple absorber layer structure is a one-dimensional (1D) n-i-p planar hetero-junction configuration, as shown in Figure 1. The simulation platform used is the Solar cell capacitance simulator (SCAPS) version 3.3.10. It is based on solving three equations including the Poisson equation, and the continuity equations for electron and holes. The equations are as follow:

Poisson equation: $-\frac{\partial}{\partial x}\left(-\varepsilon(x)\frac{\partial V}{\partial x}\right) = q[p(x) - n(x) + N_D^+(x) - N_A^-(x) + p_t(x) - n_t(x)]$ (i)

Continuity equation for the hole: $\frac{\partial p}{\partial t} = \frac{1}{q}\frac{\partial J_p}{\partial x} + G_P - R_p$ (ii)

Continuity equation for electron: $\frac{\partial n}{\partial t} = \frac{1}{q}\frac{\partial J_n}{\partial x} + G_n - R_n$ (iii)

Where q is the charge, ε is the dielectric permittivity, V is the potential, $p(x)$ is the free holes concentration, $n(x)$ is the free electrons concentration, $N_D^+(x)$ is the ionized donor concentration, $N_A^-(x)$ is the ionized acceptor concentration, $p_t(x)$ is the hole trap density, $n_t(x)$ is the trap density of electron, J_n is the current density of electron, J_p is the current density of hole, G_n is the electrons generation rate, G_p is the holes generation rate, R_n is the recombination rate of an electron, R_p is the recombination rate of the hole.

In the single absorber layer structures, we used Pb-free inorganic Cs_2TiBr_6, Cs_2TiCl_6, and Cs_2TiI_6 as photoactive layers, inorganic n-IZGO as ETL, and inorganic p- $CuSbS_2$ as HTL. In the double absorber layer structures, we have used Cs_2TiBr_6/Cs_2TiCl_6, Cs_2TiCl_6/Cs_2TiI_6, and Cs_2TiBr_6/Cs_2TiI_6 as photoactive layers. In the triple absorber layer structures, we have used $Cs_2TiBr_6/Cs_2TiCl_6/Cs_2TiI_6$ as photoactive layers. The basic n-i-p structure of the proposed simulation is depicted in Figure 1. Table 1 summarizes the input values extracted from literature and theories for SCAPS-1D numerical simulation using the data in references [13-16]. In these simulations, the interface defect layers are also important to consider.

Table 1 Input parameters of the CsTi-based PSCs

Properties	$CuSbS_2$ (HTL)	Cs_2TiBr_6	Cs_2TiCl_6	Cs_2TiI_6	IZGO (ETL)	FTO
Thickness (nm)	350	1000	1000	800	30	500
E_g (eV)	1.580	1.6	2.23	1.8	3.050	3.2
χ (eV)	4.200	4.470	4.00	3.98	4.16	4.4
N_V ($1/cm^3$)	1×10^{18}	2.14×10^{19}	1×10^{19}	1×10^{18}	5×10^{18}	1.8×10^{18}

N_C (1/cm^3)	2.×10^{18}	6×10^{19}	1×10^{19}	1×10^{19}	5 ×10^{18}	2.2 ×10^{18}
μ_e (cm^2/Vs)	4.9 ×10^1	4.4 ×10^0	4.4 ×10^0	4.4 ×10^0	1.5×10^1	2 ×10^1
μ_p (cm^2/Vs)	4.9 ×10^1	2.5 ×10^0	2.5 ×10^0	2.5 ×10^0	2 ×10^{-1}	1 ×10^1
N_D (1/cm^3)	0	10^{19}	10^{19}	10^{14}	10^{18}	10^{19}
N_A (1/cm^3)	10^{20}	10^{19}	10^{19}	10^{16}	0	0
N_T (1/cm^3)	10^{18}	10^{10}	10^{10}	10^{10}	10^{15}	10^{14}

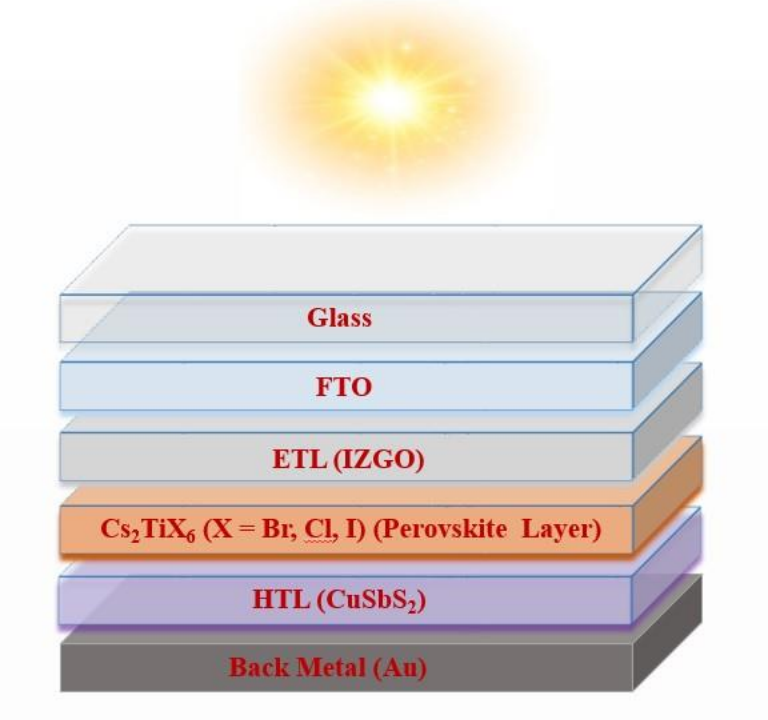

Figure 1. schematic diagram of the proposed n-i-p structure

We have used the optimized thickness in the simulated structures in previous work of ETL and HTL. In the current device, HTL is connected to the back metal contact and the ETL to a transparent conductive oxide ITO. It should be noted that the construction is illuminated by an AM1.5G solar spectrum with the density of incident power 100 mW/cm^2.

3 Results and discussion

3.1 Optimization of Single Perovskite Layer Solar Cell

3.1.1 Effect of perovskite thickness on the performance

The perovskite layer is formed of Ti-based absorber material in solar cell devices and plays a vital role in cell performance. The thin film thickness of the absorber material is essential in optimizing device efficiency. Equilibration of photo-generated holes and electrons via known recombination and absorption should be achieved. It is essential to perform an optimization procedure for the absorber thickness in a PSC. We have fixed the thickness of ETL (20 nm) and HTL(200 nm).

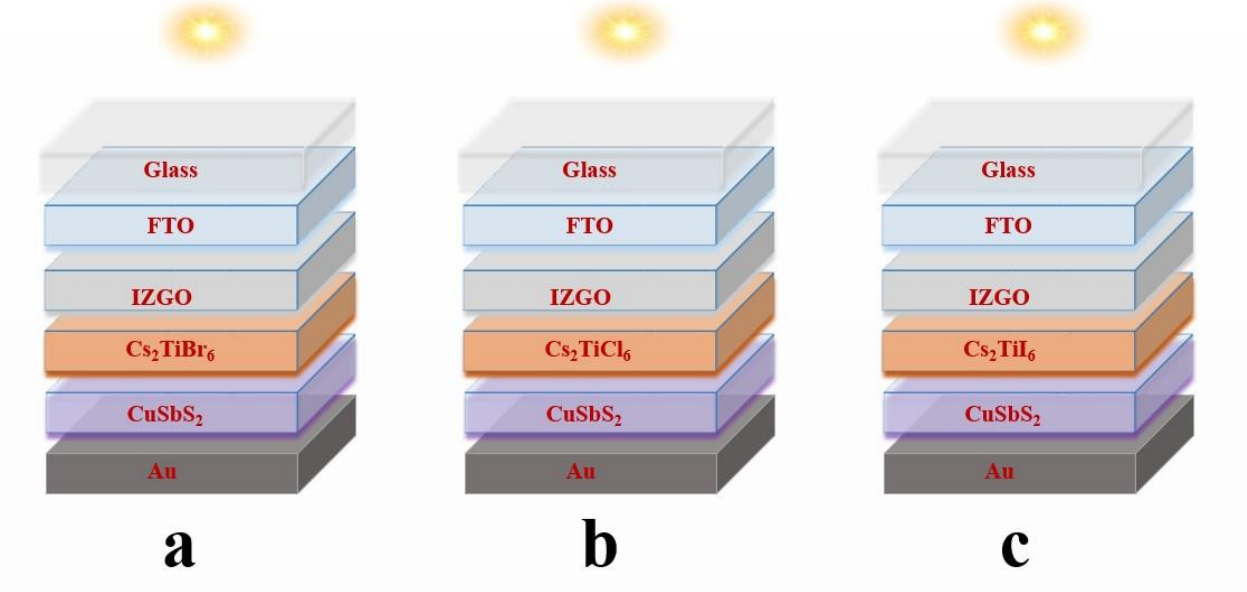

Figure 2. schematic diagram of the single absorber layer perovskite structure.

In the current simulation, to boost the device efficiency of single perovskite layer PSCs, we have changed the thickness of the single perovskite layer from 0.1 μm to 1.0 μm. The JV and QE characteristics of the three different single-layer structures are shown in Figure 3. The IV parameters, such as V_{OC}, J_{SC}, FF, and PCE have been determined with a variation of thickness, as depicted in Figure 4. The V_{OC} value increases with the rising absorbing layer thickness in Cs_2TiBr_6 and Cs_2TiCl_6 but slightly decreases in the Cs_2TiI_6 structure. The decrement in V_{OC} is due to the more carriers recombination rate. The V_{OC} value increases in the Cs_2TiBr_6 and

Cs_2TiCl_6 structures due to the improvements in recombination. The results of all structures reveal that J_{SC} grows with the layers thickness, which shows the maximum current density at 1.0 μm thickness. This indicates that the high generation of hole-electron pairs with more photon absorption can be achieved at the maximum thickness for the simulations performed. The Voc and J_{SC} values linearly increase with the perovskite layer thickness due to the increasing ration between carrier density versus recombination rate. This is clear since the V_{OC} is dependent on the device's dark saturation current and the photo-generated current, as stated in equation 1 [17].

$$V_{OC} = \frac{nkT}{e} \ln\left[\frac{J_{SC}}{J_o} - 1\right] \quad \text{(iv)}$$

Where n = ideality factor, nkT/e = thermal voltage, J_{sc} = current density from the light generator, J_o = dark saturation current. The J_o depends on the charge carrier recombination rate in the cell. The FF value has slightly reduced with the perovskite layer thickness rising due to high shunt conductance and series resistance. The non-linear behavior of V_{OC} and FF with absorber layer thickness is due to two main reasons, the presence of carrier trapping centers in the absorber layer and the changing of the bandgap profile. The PCE values of all structures increase with the perovskite layer due to the reduced carrier recombination rate. We have optimized the high efficiency in all the structures with a single absorber layer at 1.0 μm, which are follows: for the Cs_2TiBr_6 structure V_{OC} = 1.17 V, J_{SC} = 24.27 mA/cm^2, FF = 84.45 % and PCE = 24.09 %. In the Cs_2TiCl_6 structure V_{OC} = 1.94 V, J_{SC} = 9.23 mA/cm^2, FF = 57.45 % and PCE = 10.31 %. And alst in the Cs_2TiI_6 structure V_{OC} = 1.18 V, J_{SC} = 17.98 mA/cm^2, FF = 76.20 % and PCE = 16.17%.

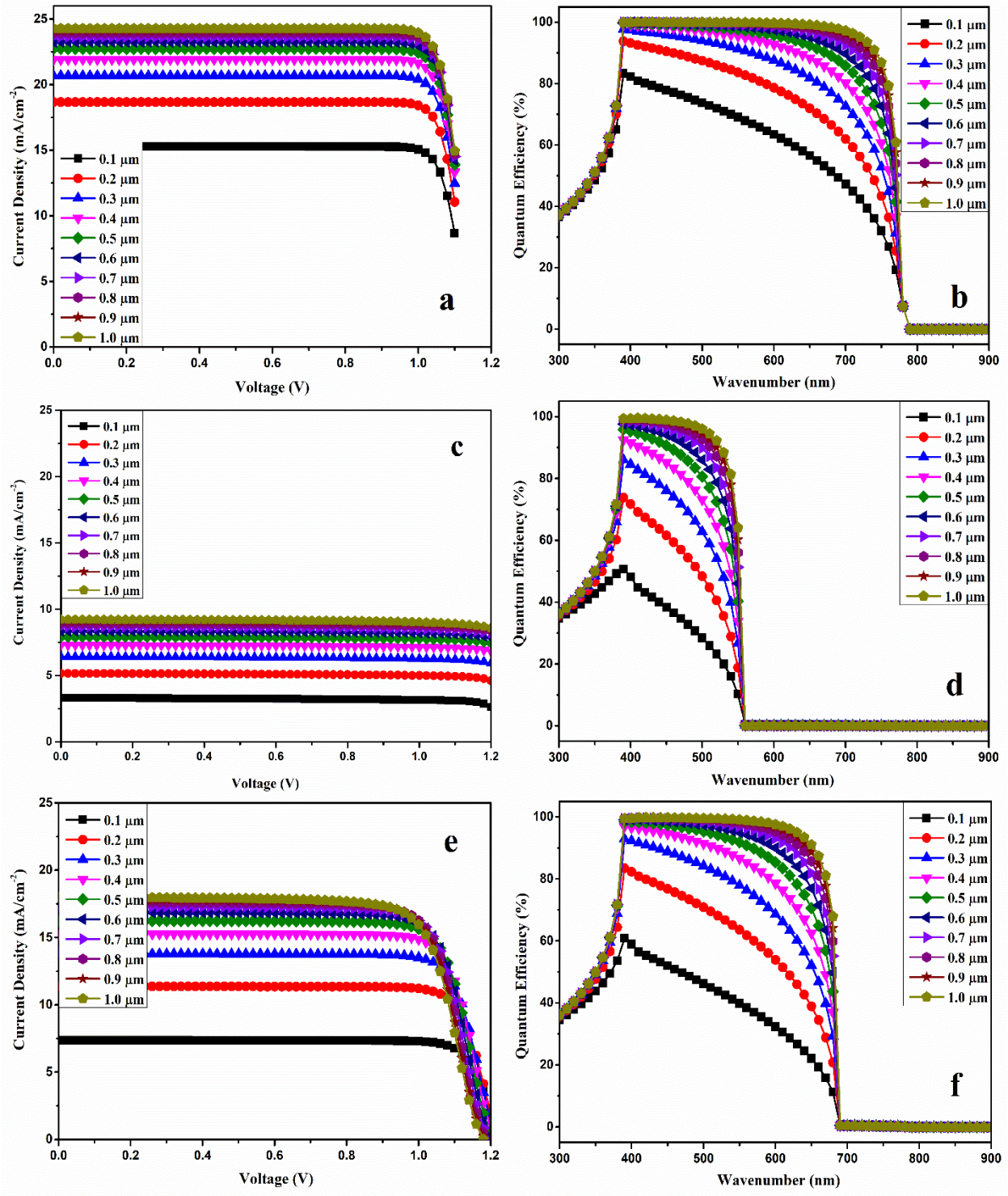

Figure 3 JV and QE characteristics of the single layer perovskite $Cs_2T_iX_6$ (X = Br, Cl, I) such as (a & b) JV and QE of $Cs_2T_iBr_6$ (c & d) JV and QE of $Cs_2T_iCl_6$ (e & f) JV and QE of $Cs_2T_iI_6$

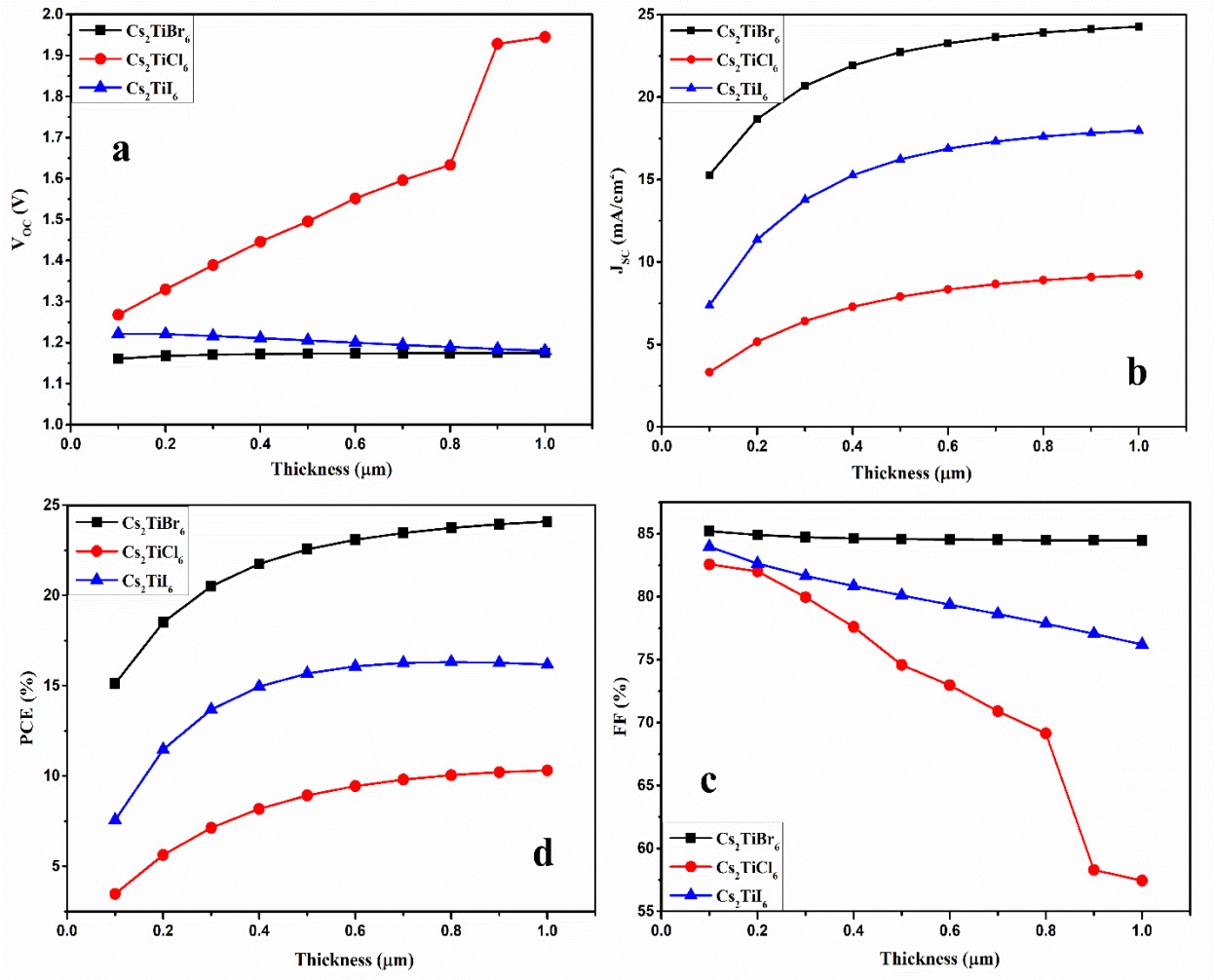

Figure 4. IV parameters of the thickness of single layer perovskite $Cs_2T_iX_6$ (X = Br, Cl, I) solar cell

3.1.2 Effect of acceptor and donor defect density on the performance

A p-type absorber layer with acceptable optoelectronic characteristics is very desirable. We will delve further into the p-type absorber characteristics that impact the performance of the proposed device. We study how the p-type perovskite doping concentration impacts the device performance of Lead-free PSC since performance may be improved by controlling doping concentration. Figure 5 shows the dependence of the IV parameters of the device for different acceptors doping concentrations in the absorber layer in the range 10^{10}-10^{22} cm^{-3}.

The Auger recombination can be highly significant when the doping density is high (>10^{19} cm^{-3}). The internal electric field of the devices can also increase with doping density. A strong internal electric field enhances the solar cell performance and the separation of photo-generated carriers. Nevertheless, high doping levels cause Auger recombination to rise and V_{oc} to drop. Due to this, the highest doping level in the photo-absorber layer in our simulation was fixed at 10^{19} cm^{-3}. Furthermore, extremely high p-type doping levels in the absorber layer can restrict hole transport from the perovskite to the HTL due to increased impurity scattering and recombination rate in the absorber layer. For further simulation, we used the acceptor density for the absorber Cs_2TiBr_6 & Cs_2TiCl_6 layers of 10^{19} cm^{-3}, and for the absorber (Cs_2TiI_6) layer we chose 10^{16} cm^{-3}.

After optimizing the acceptor doping density value of the absorber layer, we changed the donor doping concentration of the perovskite layer. Figure 6 depicts the variation of IV parameters of the solar cell for various donor doping concentrations in the perovskite layer in the range 10^{10}-10^{22} cm^{-3}. All the IV parameter values remain the same with increasing the N_D value from 10^{10} to 10^{17} cm^{-3}. The IV parameters value variates with a further increase in the N_D value due to recombination and scattering processes. The recombination rate increase with increasing the N_D value from 10^{19} cm^{-3}. In Figure 6, the fill factor value abruptly increases with an increase in donor defect density, which may be due to the non-linear behavior of the solar cell at high N_D value. This could occur if the increased donor defect density causes a shift in the maximum power point to a higher voltage, while the V_{oc} and J_{sc} also slightly vary. In this case, the fill factor values have increased, even though the overall efficiency of the solar cell have reduced due to increased recombination losses. We have optimized the N_D value of 10^{12} cm^{-3} for all the structures. For further simulation, we used the optimized N_A and N_D values.

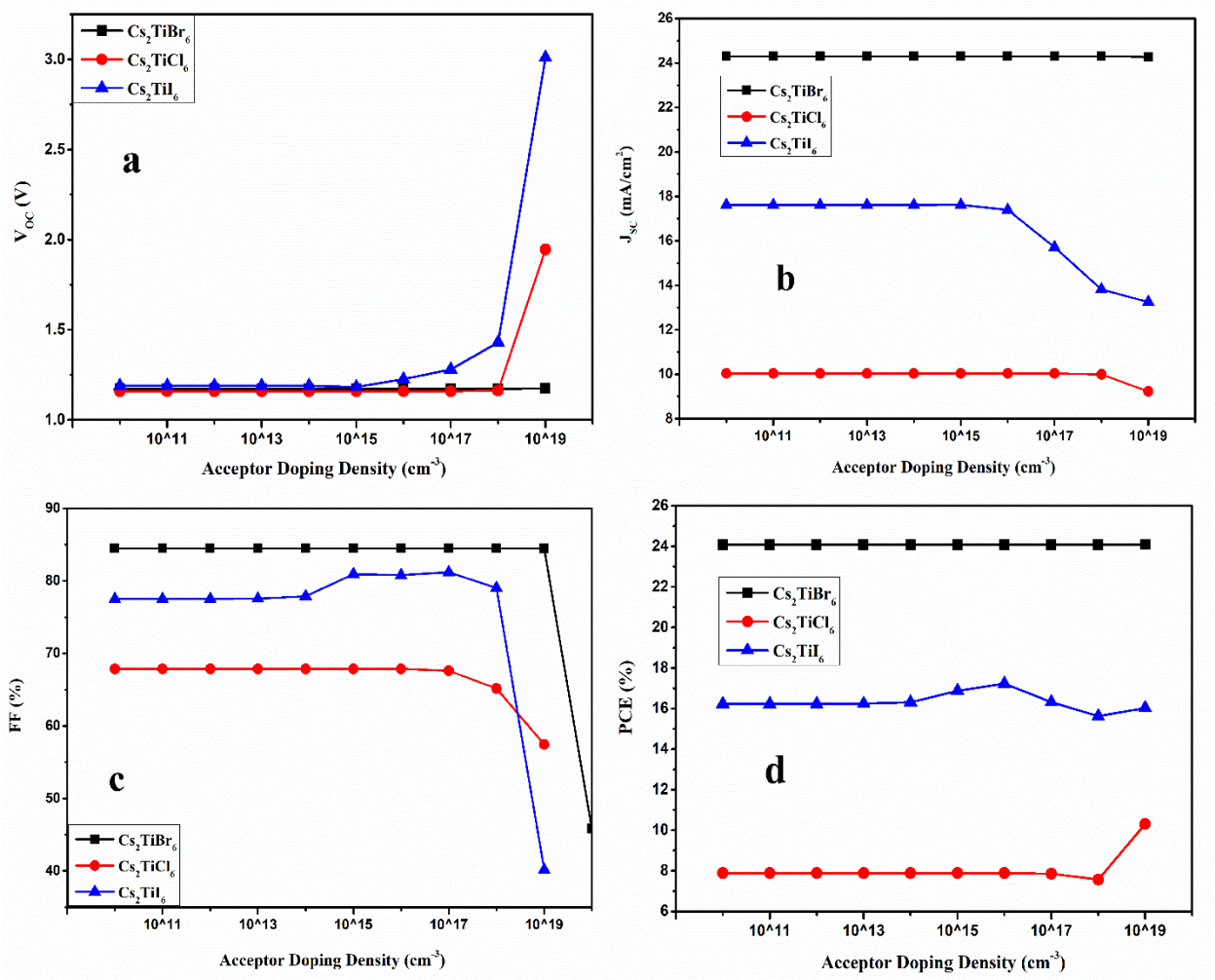

Figure 5 the acceptor defect density of a single absorber $Cs_2T_iX_6$ (X = Br, Cl, I) solar cell

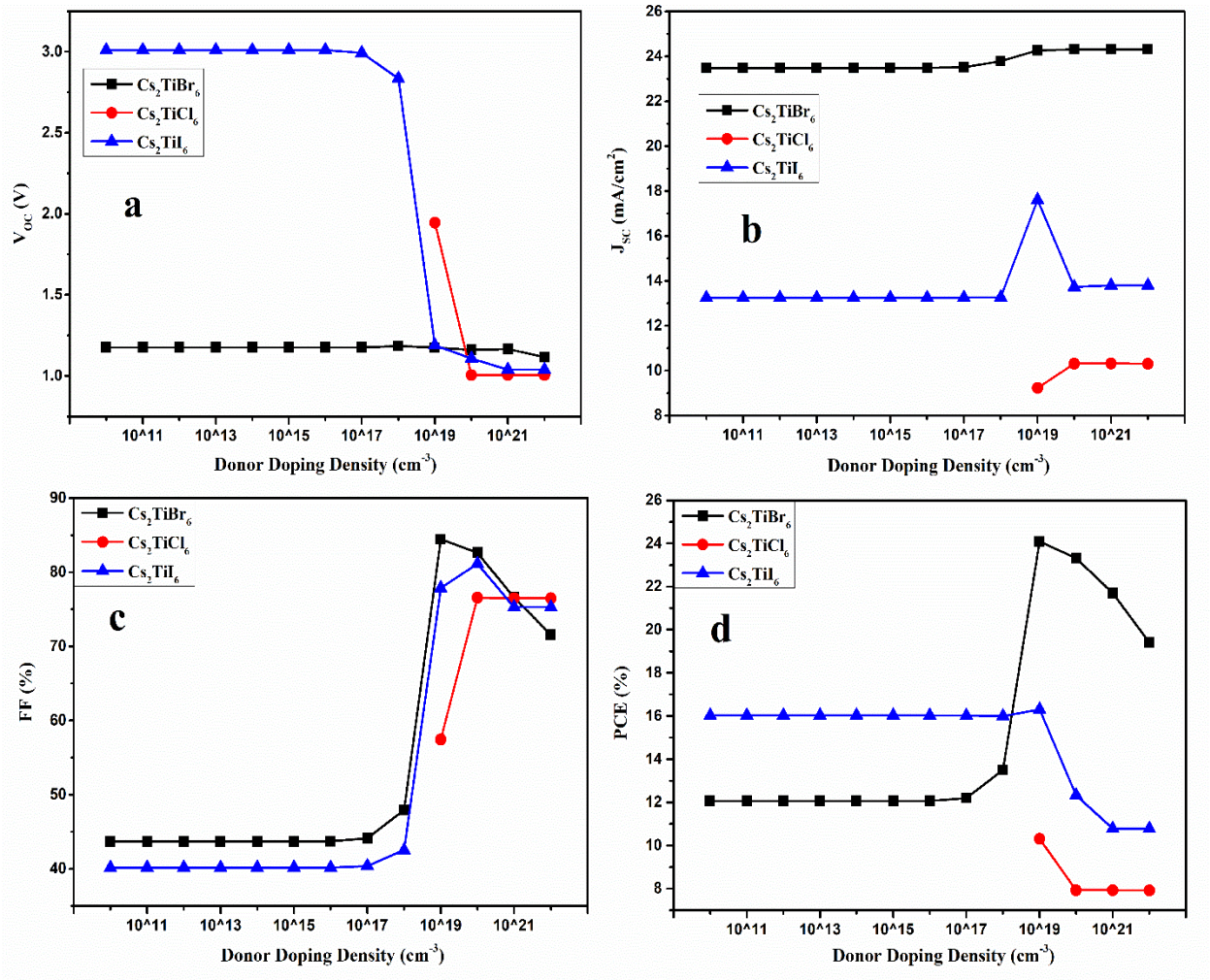

Figure 6 the donor defect density of a single absorber $Cs_2T_iX_6$ (X = Br, Cl, I) solar cell

3.1.3 Effect of defect density on the performance

The absorption, recombination and generation process in the perovskite layer depends on the defect density and quality of the film. Figure 7 depicts the fluctuation in IV parameters with changing the defect density (N_t) of all the single absorber layer perovskite solar cells. The N_t of perovskite is the primary cause of carrier recombination rate, which reduces the efficiency of PSCs and hence limits the scope of attaining the Shockley-Queisser limit [18]. According to the Shockley-Read-Hall or Trap-aided theory, recombination is the major source of the loss process in PSCs [19]. It may be lowered by enhancing the quality of the absorber layer, reducing grain

boundaries, and passivating the defect traps at the surface or bulk of the absorber layer, which is directly related to the crystallization rate during the formation of the layering process [20]. The Shockley-Read Hall recombination can be expressed by equations (v) and (vi), where σ_n and σ_p represent the capture cross sections of electrons and holes, V_{th} represents thermal velocity, E_t represents the N_t level of the trap state, and E_i represents the intrinsic level of energy [18].

$$R^{SRH} = \sigma_{n,p} V_{th} N_t \left[\frac{n_p + n_i^2}{n + p + 2n_i \cos\left({}^{E_t - E_i}/_{KT}\right)} \right] \quad \text{(v)}$$

$$L = \sqrt{D \times \tau} \quad \text{(vi)}$$

Where,

$$D = {}^{K_B T}/_{q} \times \mu \quad \text{(vii)}$$

$$\tau = {}^{1}/_{\sigma V_{th} N_t} \quad \text{(viii)}$$

Where, L is the diffusion length and depends on the D and τ. Equations (vii) and (viii) show that the increasing N_t causes a high charge recombination rate. The increase in carrier recombination is related to a decrease in diffusion length in the perovskite layer. The V_{oc}, FF and PCE values reduce with the rising N_t value. The J_{sc} value remains constant until 10^{16} cm^{-3} of all the structures due to the internal electric field, then decreases with the N_t value. Enhancing the carrier recombination rate reduces carrier lifetime, decreasing device performance. Then we used the acceptable range value (10^{10} cm^{-3}) of N_t in all structures. This number sets an important device manufacturing constraint. Researchers working on manufacturing Pb-free perovskite absorbers thus must aim to obtain materials with at least this range of defect densities.

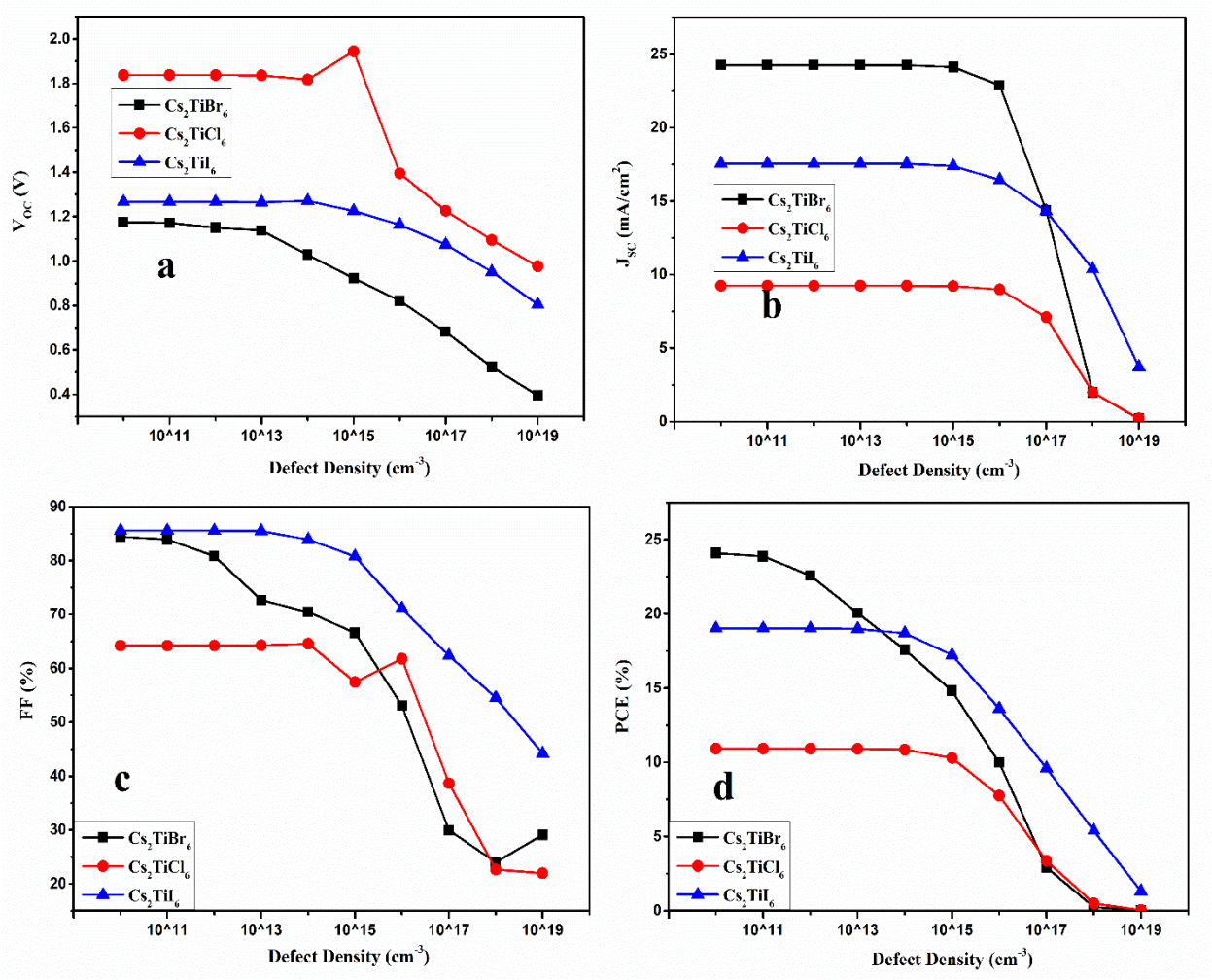

Figure 7 fluctuation of IV parameters with changing the defect density of single absorber $Cs_2T_iX_6$ (X = Br, Cl, I) solar cell

3.1.4 Interface layer defect density

We have added the interface defect density between $CuSbS_2$/perovskite and Peroveskite/IZGO layers in all the single absorber layer structures for a more realistic structure. The interface defect densities impact the stability of PSCs and efficiency. We have simulated the PSCs performance by varying interface defect density between $CuSbS_2$/perovskite and Peroveskite/IZGO layer from 10^{10} cm^{-3} to 10^{20} cm^{-3} to estimate the effect of the interface layer on the device efficiency. We have considered the defect position at the interface layer with uniform energy distribution. Figure

8 shows the cell performance by changing the $CuSbS_2$/absorber layer defect density interface layer for all single perovskite layer structures. All the IV parameters for the $Cs_2T_iX_6$ (X = Cl, I) perovskite solar cell structure remain constant for all the values except the variation of V_{OC} and FF values for $Cs_2T_iCl_6$ at 10^{15}, 10^{19} and 10^{20} cm^{-3}. The IV parameters for the $Cs_2T_iBr_6$ PSC structure decrease with increasing the interface defect density. The decrement of the device efficiency with raising the interface defect caused to trapping, scattering and recombining of holes at the interfaces during the travelling $CuSbS_2$ to the perovskite layer. We have used the 10^{10} cm^{-3} interface defect density between $CuSbS_2$/Cs_2TiBr_6 layers for further simulation. We have used the 10^{14} cm^{-3} interface defect density between $CuSbS_2$/ $Cs_2T_iX_6$ (X = Cl, I) layers for further simulation.

Figure 9 shows the cell performance with changing the interface layer of absorber/IZGO layer defect density for all single absorber layer structures. All the IV parameters for the $Cs_2T_iX_6$ (X = Br, Cl, I) perovskite solar cell structure exponentially decrease with raising the defect density. The decrement of all single absorber layer device efficiency with increasing the interface defect is caused by trapping, scattering and recombining of an electron at the interfaces during travelling perovskite to IZGO layer. We have used the 10^{10} cm^{-3} interface defect density between perovskite/IZGO layers for further simulations. We have simulated the following results with optimization of interface layer density in Cs_2TiBr_6 structure V_{OC} = 1.175 V, J_{SC} = 24.27 mA/cm^2, FF = 84.45 % and PCE = 24.09 %. In Cs_2TiCl_6 structure V_{OC} = 1.84 V, J_{SC} = 9.25 mA/cm^2, FF = 64.24 % and PCE = 10.93 %. In Cs_2TiI_6 structure V_{OC} = 1.27 V, J_{SC} = 17.55 mA/cm^2, FF = 85.6 % and PCE = 19.03%. Once again, the values of allowable defect densities found here should indicate the requirements for experimental material manufacturing.

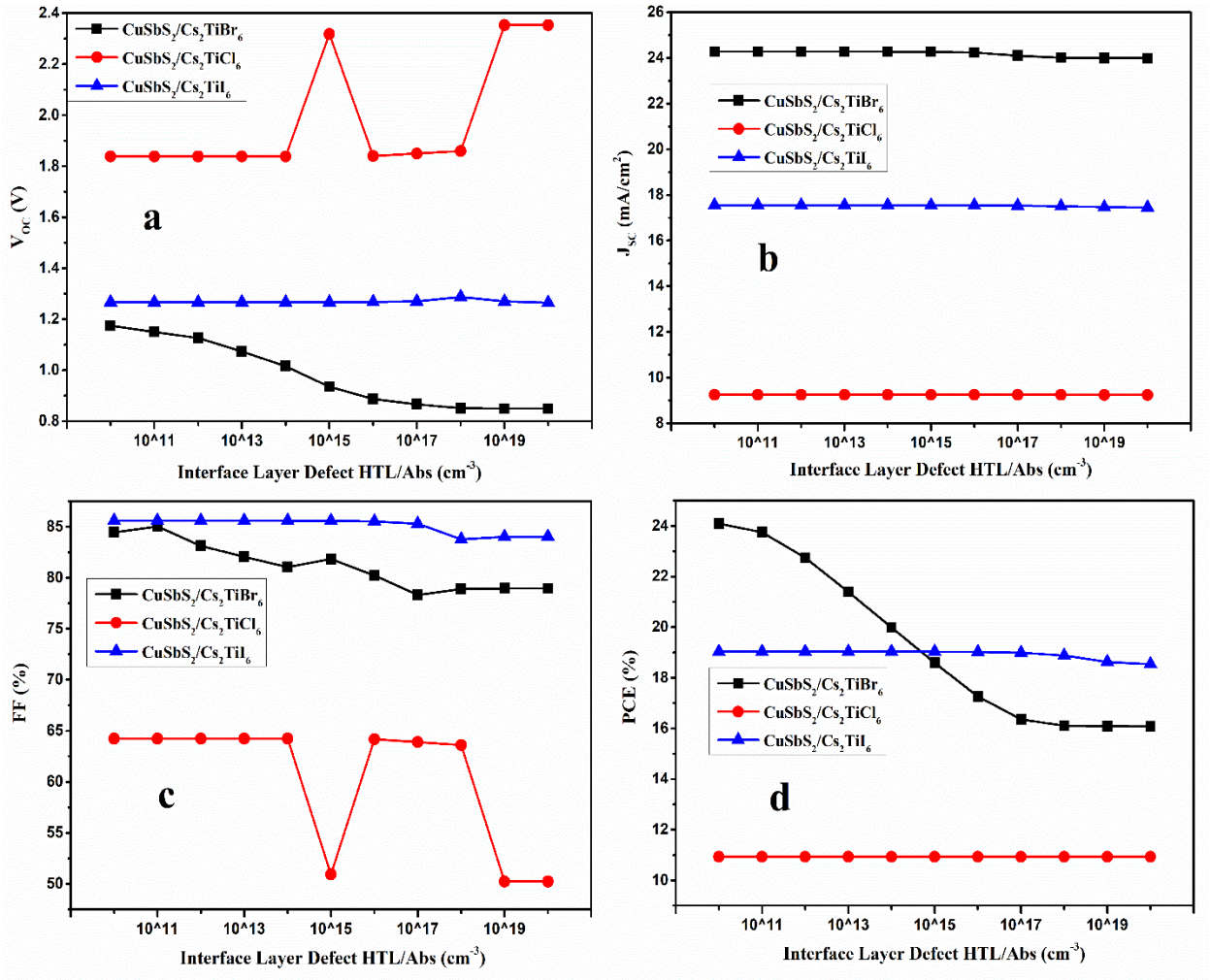

Figure 8 illustrates the fluctuation of cell performance with the defect density of the interface layer between HTM and the Peroveskite layer

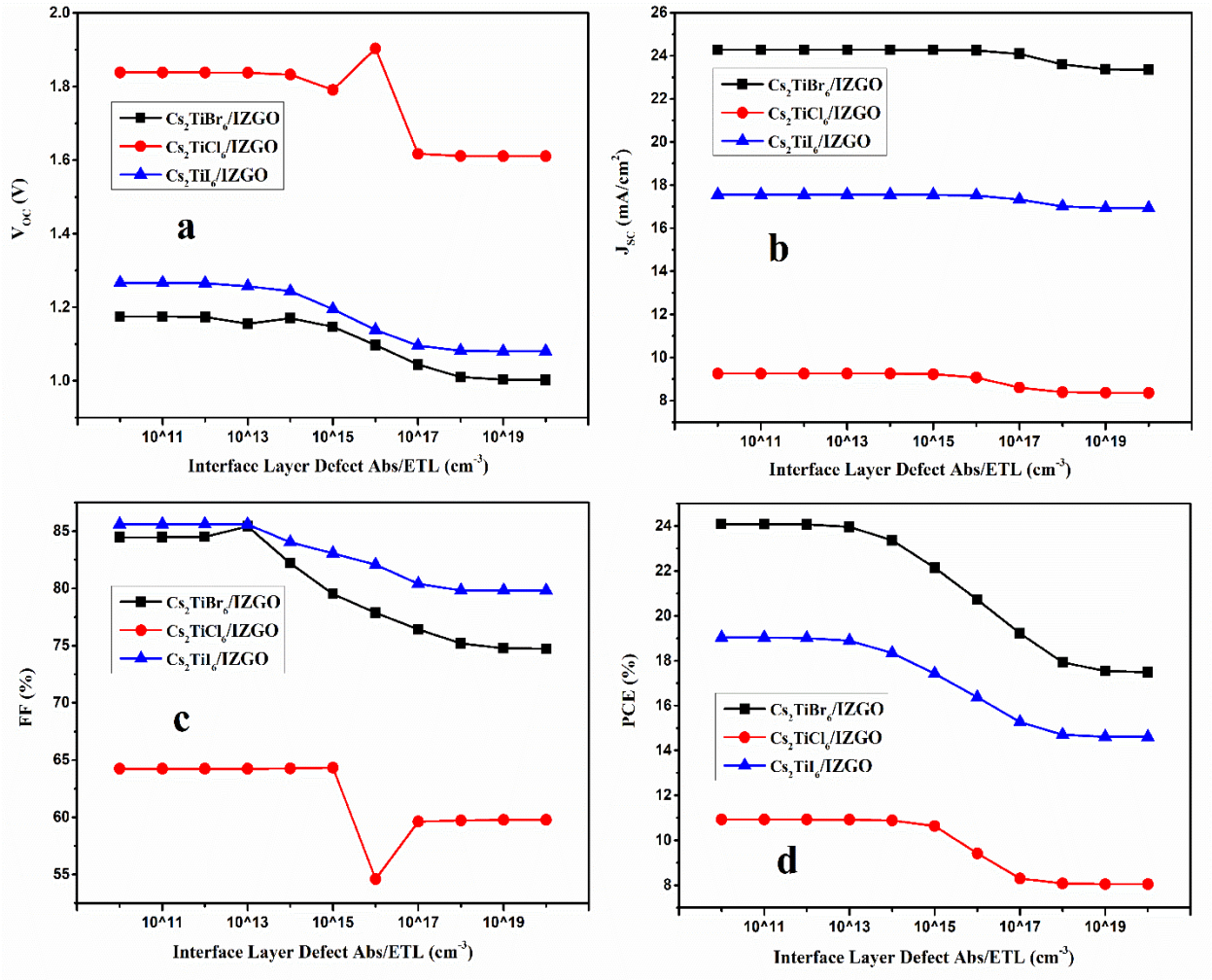

Figure 9 illustrates the fluctuation of device efficiency with the defect density of the interface layer between the Peroveskite layer and IZGO

3.1.5 Metal back contact

Figure 10 shows the fluctuation of the IV parameters of the cell using the different back metal contact with work function from 5.1 to 5.9 eV. The V_{oc} value decreased from Au (5.1) to Ni (5.5) for the structure using the C_2TiCl_6 absorber layer. But the V_{oc} value increases from Au (5.1) to Ni (5.5) for the structures using C_2TiBr_6 & C_2TiI_6 absorber layer. All the IV parameters remain constant with changing the back metal contact from Ni (5.5) to Se (5.9). The maximum performance of all structures for high metal work metal function is due to the reduction in

reverse saturation current from the increased field effect and extraction provided by the high WF. The holes easily move towards the HTM to back contact, causing the reduction of the reverse saturation current [13]. The high metal work function materials are not chemically reacted with the $CuSbS_2$ and perovskite layer. We have optimized the maximum PSC performance with the high work metal function of back contact, which is greater than 5.5 eV. We can use any back metal contact such as Ni, Pd, Pt, Se.

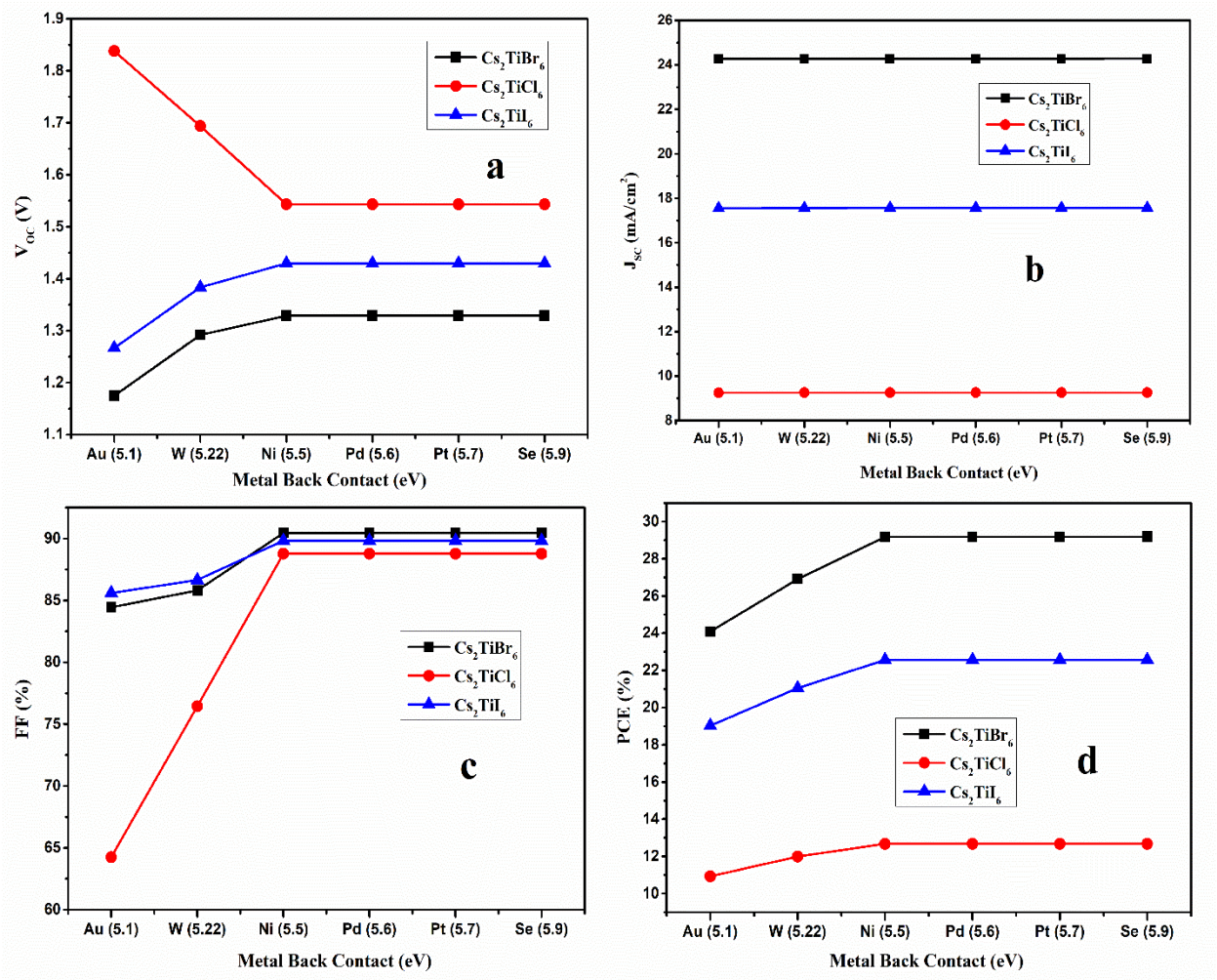

Figure 10 illustrates the fluctuation of IV parameters with different back contact metal work function

3.1.6 Temperature dependent performance

To understand the effect of environmental temperature on device performance, the external temperature of the optimum device structure is adjusted from 300 K to 420 K. Figure 11 shows the linear fluctuation of IV parameters at different temperatures. It is observed that efficiency and device performance steadily decline with increasing temperature, consistent with previous results [16]. The loss in performance of perovskite materials at higher temperatures can be attributed to the temperature dependence of material parameters, such as the recombination rate, bandgap, and absorption coefficients. As the temperature increases, the recombination rate of charge carriers in the material also increases, leading to a decrease in the efficiency of the material. In addition to the recombination rate, other material parameters such as mobility and carrier concentration may also be temperature-dependent and contribute to the loss in performance. As the external temperature rises, so does the stress deformation, which affects the performance of the device. The high temperature influences the diffusion length and results in the series resistance rising, lowering the FF and PCE of the solar cell [21].

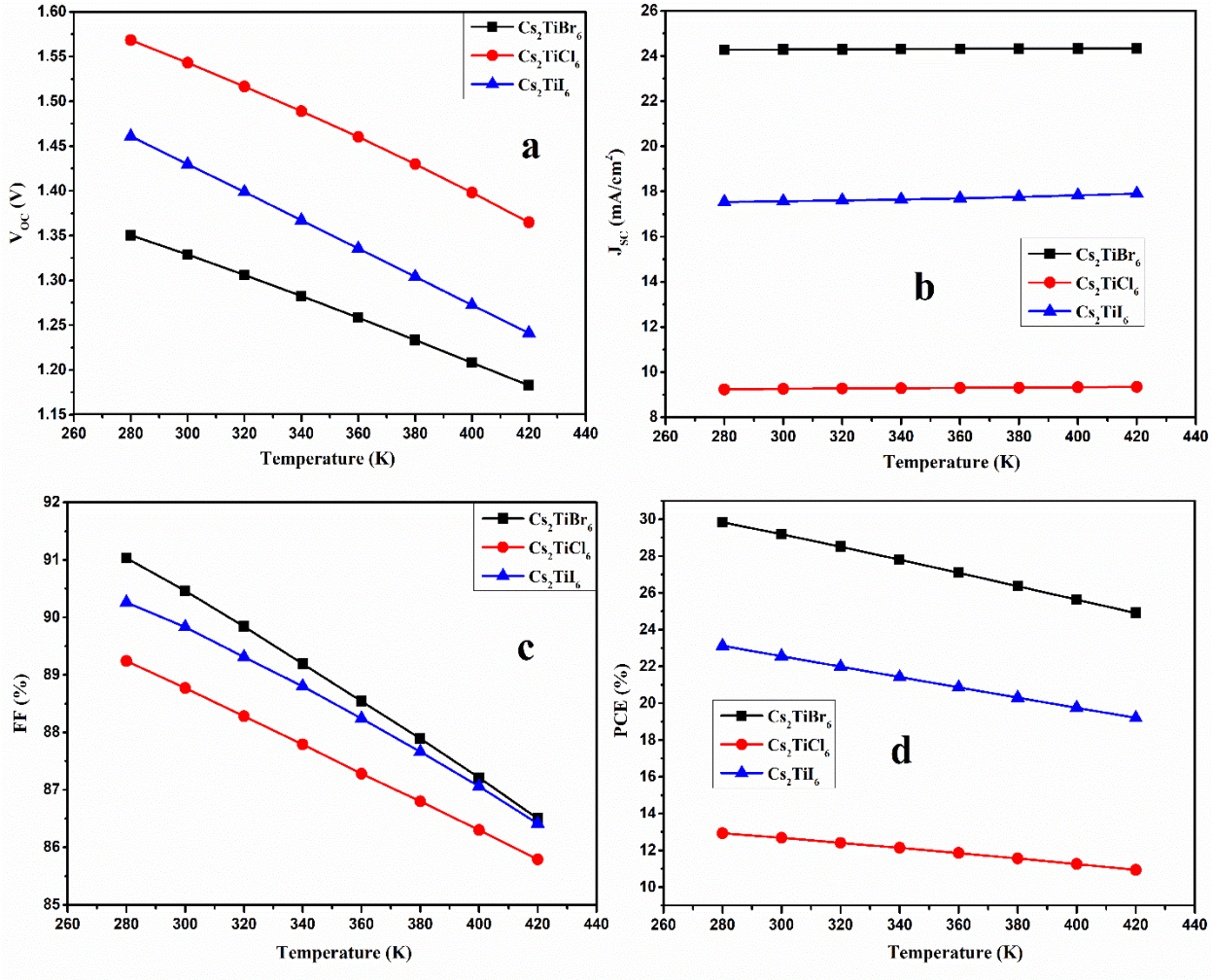

Figure 11 illustrates the linear fluctuation in IV parameters with changing the temperature

Finally, we have optimized the physical parameters of a single absorber layer perovskite structure with maximum efficiency. In all the CsTi-based perovskite solar cell structures, we have improved the best absorber layer thickness, absorber and donor density of the absorber layer, defect density and interface $CuSbS_2$/absorber and absorber/IZGO defect density. We have optimized the efficiency of the single absorber layer structure in Cs_2TiBr_6 structure V_{OC} = 1.33 V, J_{SC} = 24.28 mA/cm^2, FF = 90.46 % and PCE = 29.19 %. In Cs_2TiCl_6 structure V_{OC} = 1.54 V, J_{SC} = 9.26 mA/cm^2, FF = 88.77 % and PCE = 12.68 %. In Cs_2TiI_6 structure V_{OC} = 1.43 V, J_{SC} = 17.57 mA/cm^2, FF = 89.83 % and PCE = 22.56 %.

3.2 Optimization of Double Perovskite Layer Solar Cell

We have studied the double PSCs structure as shown in the schematic diagram in figure 12. We have simulated three structures with a double perovskite layer. In these double perovskite structures, we have added the already optimized parameters. For further optimization, we have simulated the interface defect density between double perovskite from 10^8 to 10^{15} cm^{-3}. Figure 13 depicts the fluctuation in IV parameters with varying interface density between perovskite layers. The solar cell performance remains the same with increasing interface density. We have optimized the interface defect density value 10^{14} cm^{-3} for all three structures with double perovskite. We have optimized the efficiency of the double absorber layer structure in FTO/IZGO/Cs_2TiBr_6/Cs_2TiCl_6/$CuSbS_2$/Se structure V_{OC} = 1.54 V, J_{SC} = 24.04 mA/cm^2, FF = 82.72 % and PCE = 30.06 %. In FTO/IZGO/Cs_2TiBr_6/Cs_2TiI_6/$CuSbS_2$/Se structure V_{OC} = 1.37 V, J_{SC} = 24.10 mA/cm^2, FF = 84.55 % and PCE = 28.05 %. In FTO/IZGO/Cs_2TiCl_6/Cs_2TiI_6/$CuSbS_2$/Se structure V_{OC} = 1.43 V, J_{SC} = 17.53 mA/cm^2, FF = 89.52 % and PCE = 22.49 %. The efficiency increases with the double perovskite structure due to increased absorption with different band gap layers.

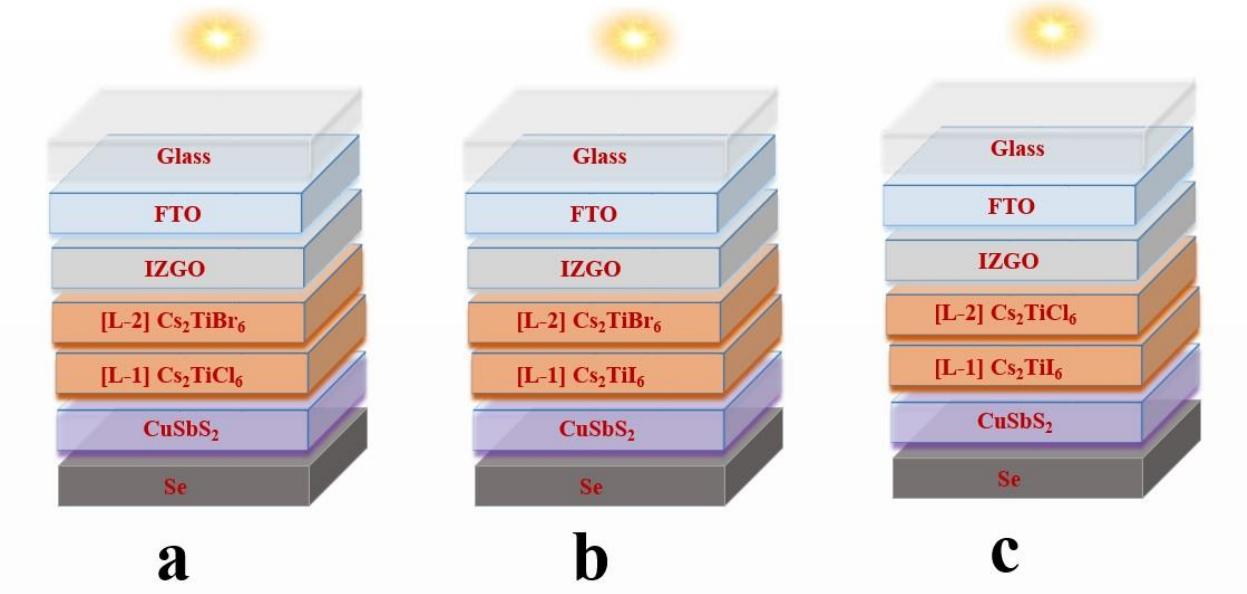

Figure 12. schematic diagram of double perovskite solar cell (a) Cs_2TiBr_6/Cs_2TiCl_6 (b) Cs_2TiBr_6/Cs_2TiI_6 (c) Cs_2TiCl_6/Cs_2TiI_6

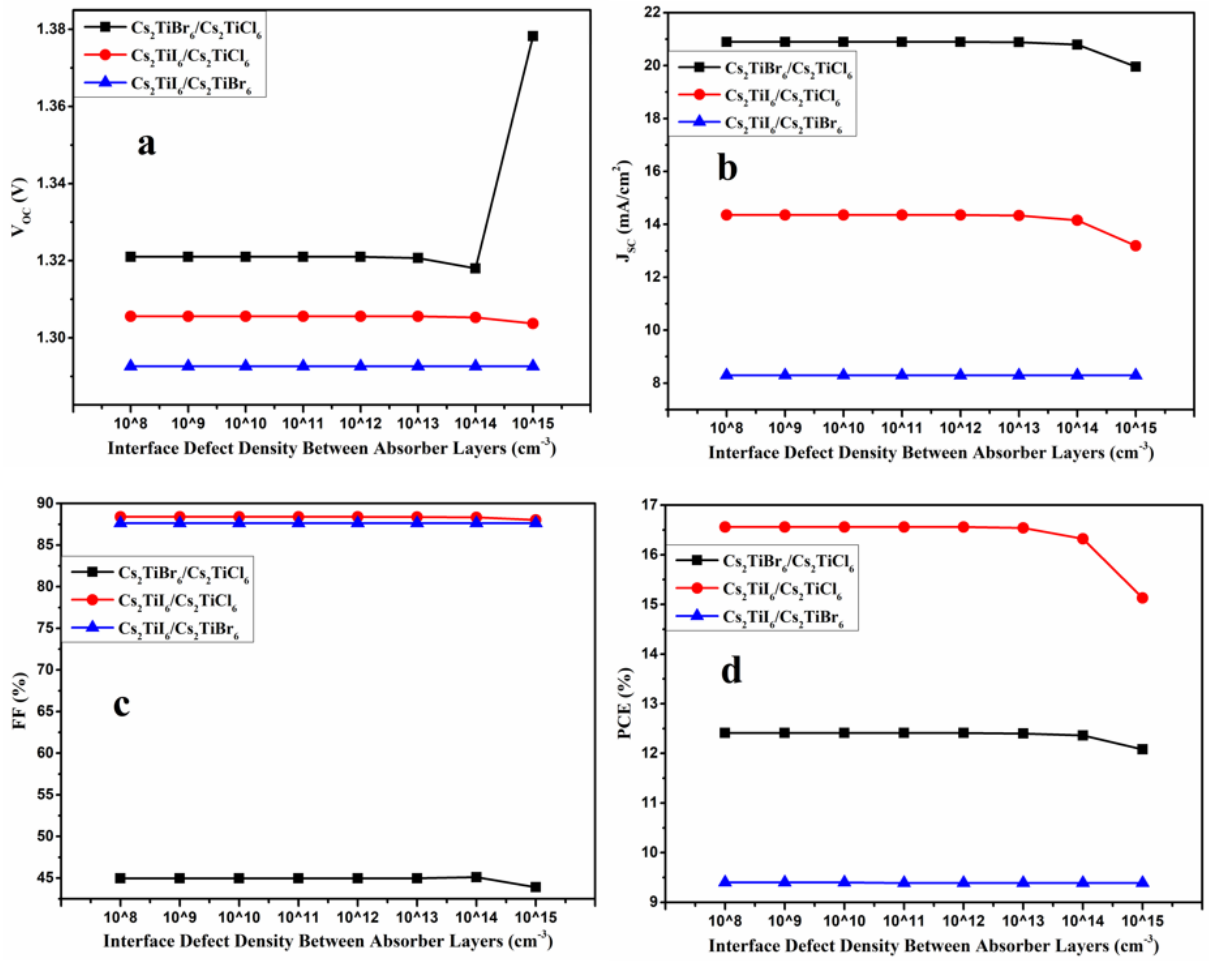

Figure 13 IV parameters of the double PSC by varying the interface defect density between both absorber layer

3.3 Optimization of Tripple Perovskite Layer Solar Cell

As shown in the inset schematic diagram, we have numerically simulated the triple PSC structure. The JV and QE properties of triple absorber layer PSC are shown in figure 14. We have simulated the triple perovskite solar cell structure with absorber layer $Cs_2T_iX_6$ (X = Br, Cl, I). We have already used optimized parameters such as absorber and donor defect density of the perovskite layers and interface defect density. We have numerical simulated the following

FTO/IZGO/Cs_2TiBr_6/Cs_2TiCl_6/Cs_2TiI_6/$CuSbS_2$/Se structure: the V_{OC} = 1.61 V, J_{SC} = 9.26 mA/cm^2, FF = 88.50 % and PCE = 13.19 %.

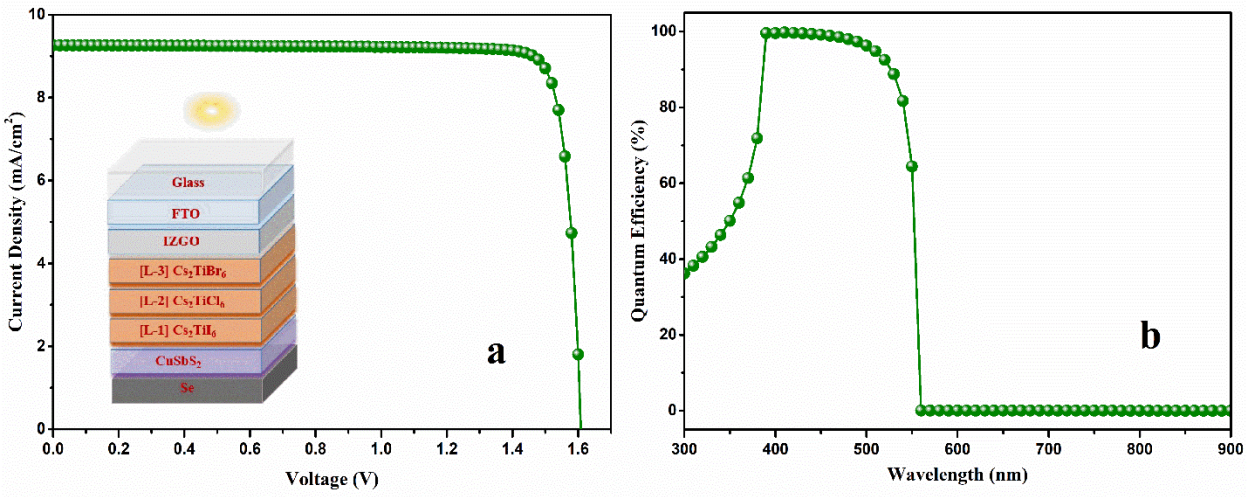

Figure 14 (a) the JV and (b) QE properties of the triple absorber layer PSC

4 Conclusion

In this study, a single, double and triple active absorber layer Cs_2TiX_6 (X = Br, Cl, I) perovskite solar cells have been simulated and analyzed using SCAPS-1D numerical simulator. $CuSbS_2$ has been used as HTL and IZGO as ETL. The PCE of more than 30 % was achieved by carefully designing the device parameters. In order to optimize efficiency, we found the suitable parameters such as the thickness of the perovskite layer, acceptor and donor defect density and defect density of the perovskite layer, interface defect density, back metal electrodes and temperature effect. We have also optimized the interface defect density between absorber layers in the double perovskite solar cell structure. This theoretical research will lay the groundwork for new approaches to developing efficient lead-free single, double and triple PSCs with maximum performance and stability. The results here will aid materials design and manufacture for future photovoltaic devices.

Acknowledgements

The authors would like to acknowledge the British Council for their funding under PAK-UK ICRG 2020 project (006327/D/ISB/008/2021) to create a research group of MS, Ph.D and Postdoctoral students and establishment of “Semiconductor Physics and Renewable Energy Laboratory” (SPREL) at Government College University Faisalabad Pakistan. R.S.B was supported by the Royal Academy of Engineering under the Research Fellowship scheme. The authors express their gratitude to Princess Nourah bint Abdulrahman University Researchers Supporting Project Number (PNURSP2023R111), Princess Nourah bint Abdulrahman University, Riyadh, Saudi Arabia.

5 References

[1] J. Burschka, N. Pellet, S.-J. Moon, R. Humphry-Baker, P. Gao, M.K. Nazeeruddin, M. Grätzel, Sequential deposition as a route to high-performance perovskite-sensitized solar cells, Nature, 499 (2013) 316-319.

[2] P. Research, Best Research-Cell Efficiency Chart, NREL, 2022.

[3] C. Lian, Z.A. Ali, H. Kwon, B.M. Wong, Indirect but efficient: laser-excited electrons can drive ultrafast polarization switching in ferroelectric materials, The journal of physical chemistry letters, 10 (2019) 3402-3407.

[4] J.H. Noh, S.H. Im, J.H. Heo, T.N. Mandal, S.I. Seok, Chemical management for colorful, efficient, and stable inorganic–organic hybrid nanostructured solar cells, Nano letters, 13 (2013) 1764-1769.

[5] Y. Yang, J. You, Make perovskite solar cells stable, Nature, 544 (2017) 155-156.

[6] D. Kong, D. Cheng, X. Wang, K. Zhang, H. Wang, K. Liu, H. Li, X. Sheng, L. Yin, Solution processed lead-free cesium titanium halide perovskites and their structural, thermal and optical characteristics, Journal of Materials Chemistry C, 8 (2020) 1591-1597.

[7] B.V. Lotsch, New light on an old story: perovskites go solar, Angewandte Chemie International Edition, 53 (2014) 635-637.

[8] H. Zhang, Y. Shi, F. Yan, L. Wang, K. Wang, Y. Xing, Q. Dong, T. Ma, A dual functional additive for the HTM layer in perovskite solar cells, Chemical Communications, 50 (2014) 5020-5022.

[9] R. Singh, P.K. Singh, B. Bhattacharya, H.-W. Rhee, Review of current progress in inorganic hole-transport materials for perovskite solar cells, Applied Materials Today, 14 (2019) 175-200.

[10] M.-G. Ju, M. Chen, Y. Zhou, H.F. Garces, J. Dai, L. Ma, N.P. Padture, X.C. Zeng, Earth-abundant nontoxic titanium (IV)-based vacancy-ordered double perovskite halides with tunable 1.0 to 1.8 eV bandgaps for photovoltaic applications, ACS Energy Letters, 3 (2018) 297-304.

[11] T. Das, G. Di Liberto, G. Pacchioni, Density functional theory estimate of halide perovskite band gap: when spin orbit coupling helps, The Journal of Physical Chemistry C, 126 (2022) 2184-2198.

[12] K. Shivesh, I. Alam, A.K. Kushwaha, M. Kumar, S.V. Singh, Investigating the theoretical performance of Cs_2TiBr_6-based perovskite solar cell with La-doped $BaSnO_3$ and $CuSbS_2$ as the charge transport layers, International Journal of Energy Research, 46 (2022) 6045-6064.

[13] S. Mushtaq, S. Tahir, A. Ashfaq, R.S. Bonilla, M. Haneef, R. Saeed, W. Ahmad, N. Amin, Performance optimization of lead-free $MASnBr_3$ based perovskite solar cells by SCAPS-1D device simulation, Solar Energy, 249 (2023) 401-413.

[14] G. Pindolia, S.M. Shinde, P.K. Jha, Optimization of an inorganic lead free $RbGeI_3$ based perovskite solar cell by SCAPS-1D simulation, Solar Energy, 236 (2022) 802-821.

[15] K. Chakraborty, M.G. Choudhury, S. Paul, Study of physical, optical, and electrical properties of cesium titanium (IV)-based single halide perovskite solar cell, IEEE Journal of Photovoltaics, 11 (2021) 386-390.

[16] K.D. Jayan, V. Sebastian, Comprehensive device modelling and performance analysis of $MASnI_3$ based perovskite solar cells with diverse ETM, HTM and back metal contacts, Solar Energy, 217 (2021) 40-48.

[17] M.A. Green, Solar cells: operating principles, technology, and system applications, Englewood Cliffs, (1982).

[18] W. Shockley, W. Read Jr, Statistics of the recombinations of holes and electrons, Physical review, 87 (1952) 835.

[19] W. Tress, N. Marinova, O. Inganäs, M.K. Nazeeruddin, S.M. Zakeeruddin, M. Graetzel, Predicting the open-circuit voltage of CH3NH3PbI3 perovskite solar cells using electroluminescence and photovoltaic quantum efficiency spectra: the role of radiative and non-radiative recombination, Advanced Energy Materials, 5 (2015) 1400812.

[20] M.A. Contreras, L.M. Mansfield, B. Egaas, J. Li, M. Romero, R. Noufi, E. Rudiger-Voigt, W. Mannstadt, Wide bandgap Cu (In, Ga) Se2 solar cells with improved energy conversion efficiency, Progress in Photovoltaics: Research Applications, 20 (2012) 843-850.

[21] F. Behrouznejad, S. Shahbazi, N. Taghavinia, H.-P. Wu, E.W.-G. Diau, A study on utilizing different metals as the back contact of $CH_3NH_3PbI_3$ perovskite solar cells, Journal of Materials chemistry A, 4 (2016) 13488-13498.